ACS APPLIED ENERGY MATERIALS

www.acsaem.org

Article

Scalable Large-Area 2D-MoS_2/Silicon-Nanowire Heterostructures for Enhancing Energy Storage Applications

Ioannis Zeimpekis, Tasmiat Rahman, Oi Man Leung, Jack Tyson, Martin Ebert, Stuart A. Boden, Carlos Ponce De Leon, and Katrina A. Morgan*

Cite This: https://doi.org/10.1021/acsaem.3c03055

Read Online

ACCESS | Metrics & More | Article Recommendations

ABSTRACT: Two-dimensional (2D) transition-metal dichalcogenides have shown great potential for energy storage applications owing to their interlayer spacing, large surface area-to-volume ratio, superior electrical properties, and chemical compatibility. Further, increasing the surface area of such materials can lead to enhanced electrical, chemical, and optical response for energy storage and generation applications. Vertical silicon nanowires (SiNWs), also known as black-Si, are an ideal substrate for 2D material growth to produce high surface-area heterostructures, owing to their ultrahigh aspect ratio. Achieving this using an industrially scalable method paves the way for next-generation energy storage devices, enabling them to enter commercialization. This work demonstrates large surface area, commercially scalable, hybrid MoS_2/SiNW heterostructures, as confirmed by Raman spectroscopy, with high tunability of the MoS_2 layers down to the monolayer scale and conformal MoS_2 growth, parallel to the silicon nanowires, as verified by transmission electron microscopy (TEM). This has been achieved using a two-step atomic layer deposition (ALD) process, allowing MoS_2 to be grown directly onto the silicon nanowires without any damage to the substrate. The ALD cycle number accurately defines the layer number from monolayer to bulk. Introducing an ALD alumina (Al_2O_3) interface at the MoS_2/SiNW boundary results in enhanced MoS_2 quality and uniformity, demonstrated by an order of magnitude reduction in the B/A exciton photoluminescence (PL) intensity ratio to 0.3 and a reduction of the corresponding layer number. This high-quality layered growth on alumina can be utilized in applications such as for interfacial layers in high-capacity batteries or for photocathodes for water splitting. The alumina-free 100 ALD cycle heterostructures demonstrated no diminishing quality effects, lending themselves well to applications that require direct electrical contact with silicon and benefit from more layers, such as electrodes for high-capacity ion batteries.

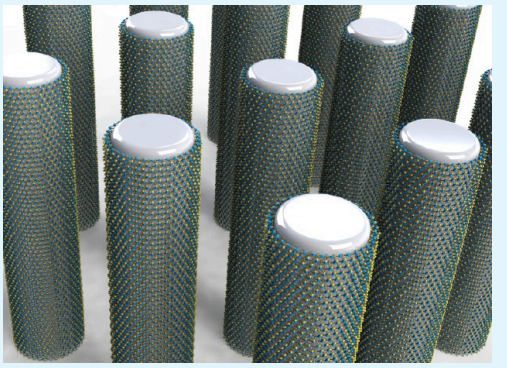

KEYWORDS: *2D materials, energy storage, MoS_2, nanowires, scalable, TMD*

INTRODUCTION

There is currently a rapidly growing demand for low-cost, high-density energy storage.[1] This is especially prevalent as the world moves toward clean energy that requires storage to be effectively deployed. This must be performed in a sustainable manner; therefore, alternative electrodes and chemistries are currently being rapidly explored. The unique chalcogen−metal−chalcogen structure of transitional-metal dichalcogenides (TMDs) gives them unique properties such as the ability to retain large numbers of ions due to their interlayer spacing[2,3] (2H-MoS_2 6.5 Å,[4] 1T-MoS_2 > 10 Å,[5] tunable through addition of elements[6,7]) and their intralayer stackable nature. TMDs can facilitate increased ionic interaction and increase electrical conduction within electrode/electrolyte interfaces in ionic batteries, leading to high-capacity batteries.[4,7,8] The ability to provide high capacity coupled with the high stability of these materials constitutes them as ideal candidates for battery electrodes and interfacial layers.[9−11] Other TMD properties including high mobility, tunable bandgap, high mechanical flexibility, high surface-to-volume ratio, and supercapacitive and catalytic activity offer unique property combinations for next-generation fuel cells[12,13] and solar cells.[13,14] Specifically, TMDs can act as power conversion efficiency enhancing layers in solar cells,[15,16] additionally increasing lifetime and dramatically reducing waste arising from solar panel replacement. TMDs can also be used in the cost-effective production of hydrogen,[11,17,18] resolving one of the most persistent stumbling blocks for its use as a clean energy source.

Received: December 7, 2023
Revised: February 27, 2024
Accepted: February 27, 2024

Table 1. Sample List with Process Steps and Aims for Each Sample

Sample name	Process steps (post SiNW growth)	Investigations
S1	No further processing	Bare SiNW for reference
S2	Anneal	H_2S anneal effects on SiNWs
S3	15 cycles of MoO_3 ALD, no anneal	MoO_3 ALD growth on SiNWs
S4	15 cycles of MoO_3 ALD + H_2S anneal	Monolayer MoS_2 growth on SiNWs
S5	100 cycles of MoO_3 ALD + H_2S anneal	Multilayer MoS_2 growth on SiNWs
S6	Al_2O_3 ALD + 15 cycles of MoO_3 ALD + H_2S anneal	Al_2O_3 interlayer for monolayer MoS_2 on SiNWs
S7	Al_2O_3 ALD + 100 cycles of MoO_3 ALD + H_2S anneal	Al_2O_3 interlayer for multilayer MoS_2 on SiNWs

The energy storage and generation potential of TMDs can be further exploited by increasing their acting surface area. This inherently enhances electrolyte/semiconductor interactions, electrolyte/electrode interactions, charge carrier transport efficiency, light-trapping phenomena, and scattering effects and thus increases performance at the device level.[19−22] High-surface-area 2D material structures have been successfully demonstrated using silicon nanowires and similar morphologies, as a scaffold.[19−22] However, due to the fabrication complexity of large-area 2D materials across high-aspect-ratio structures, accurate, commercially scalable, parallel layer growth of 2D-MoS_2 layers on silicon nanowires has not been demonstrated to date.

2D transition-metal dichalcogenides, such as MoS_2, can be produced using a variety of deposition and growth techniques including sputtering,[23,24] thermal treatments,[25,26] drop-casting,[21,27] inkjet printing,[28,29] chemical vapor deposition (CVD),[30−32] and ALD[33,34] or a combination of these. The MoS_2 layer number defines the electrical properties such as conductance and the ability to make good contacts determining the performance and application space. Direct sputtering of MoS_2 on silicon nanowires results in amorphous growth, unwanted material build-up on the tips of the wires, and vertical layer growth to the nanowire surface,[20] limiting performance. Drop-casting faces similar challenges, including inaccurate control of the number of layers.[21] CVD offers a more controllable and scalable method, producing conformal growth with parallel layers,[35] but the exposure of silicon nanowires to a harsh sulfur environment reduces the quality of the system.

To investigate the performance of high aspect ratio MoS_2-coated electrodes, we employ a scalable method to fabricate large areas of high aspect ratio silicon nanowires[36−38] (height 3.5 μm, width 100 nm) conformally coated with MoS_2 in parallel growth orientation, with no nanowire deterioration. MoO_3 is deposited by ALD to create a template and then converted to MoS_2 in a sulfur environment annealing.[39] The template layer protects the substrate, resulting in a higher-quality hybrid structure. This ALD-based method provides excellent conformity, uniformity, crystallinity, and decoupled stoichiometric and layer number control. Following our previous work, we investigate the addition of an interfacial alumina layer to further enhance the quality of subsequent layers.[40] Our large-area industrially scalable and highly controllable hybrid structure approach aims among other applications to provide high-performance electrodes for batteries[41,42] to underpin high capacity, long lifetime, and high safety. Our results include scanning electron microscopy (SEM), TEM, Raman spectroscopy, and photoluminescence to analyze the MoS_2 layer number, quality, uniformity, and interfacial effects of the alumina.

EXPERIMENTAL SECTION

To investigate the individual fabrication process step effects on the nanowire substrates and to gain understanding of the significance of the process order, we fabricated seven samples as shown in Table 1. These 2.5 × 2.5 cm SiNW samples were fabricated as described, undergoing various steps of the MoS_2 growth using our two-step process. One sample (S1) was used as a SiNW reference and underwent no further processing. Two samples underwent one of the two steps of the MoS_2 growth, separately, with one sample (S2) undergoing the hydrogen sulfide (H_2S) anneal with no prior MoO_3 growth, while the other (S3) underwent the standard 15 ALD cycles of MoO_3 growth and no anneal. Please note, throughout the manuscript, 15 and 100 cycles refer to the number of ALD cycles used to deposit the MoO_3; these numbers do not refer to the number of subsequent MoS_2 layers that have grown as a result of the process. Please see the Raman results for layer number. Two further samples underwent the full MoS_2 process, one with 15 ALD cycles of MoO_3 (S4) and one with 100 ALD cycles of MoO_3 (S5), both followed by the H_2S anneal. The last two samples (S6 and S7) underwent the same process but with an interim ALD alumina step prior to the MoO_3 growth.

Silicon Nanowire Fabrication. The fabrication process starts from cleaving an n-type silicon wafer into 2.5 cm × 2.5 cm chips. These are then cleaned using RCA1 (H_2O_2−NH_4OH−H_2O) and RCA2 (H_2O_2−HCl−H_2O) solution, as well as a Piranha Etch (H_2SO_4−H_2O_2). Following the cleaning steps, they undergo a metal-assisted chemical etch (MACE) process to form the silicon nanowires. This is a top-down process, which begins with nucleation at the surface using Ag nanoparticles, followed by etching with hydrofluoric acid.[37,38] This uses a solution of $AgNO_3$ and hydrofluoric (HF) acid and leaves grass-like nanowires, whereby the height is determined from the etch time and density from the $AgNO_3$ concentration. Post etching, the remaining Ag nanoparticles are removed using nitric acid. These silicon surfaces have ultralow broadband reflectivity (<1%) due to their high surface area (therefore referred to as black-Si) and have been utilized for energy harvesting, storage, and sensing.

Alumina Interfacial Deposition. Alumina is deposited via ALD using a Veeco Savannah S200 with TMA and water vapor as the precursors at 200 °C.

Two-Step MoS_2 Growth. MoS_2 is grown in a two-step process; the first step is an ALD MoO_3 layer, and the second step is an anneal in hydrogen sulfide (H_2S) whereby the MoO_3 is converted to MoS_2 as described in ref 39. We employed two different thicknesses of MoO_3 at the ALD stage, thus leading to two different MoS_2 layer thicknesses. This was attained by controlling the number of ALD cycles to either 15 or 100. The cycle number refers to the ALD growth mechanism, whereby one cycle involves the input and purge of two gases, leading to a self-limiting growth technique. This accurate control of the layer thickness enables uniform growth and high-quality layers.

Characterization Techniques. The characterization techniques used to assess the MoS_2 growth on silicon nanowires in this work are Raman, photoluminescence, and TEM, enabling the presence, quality, coverage, and layer number of MoS_2 to be confirmed, and SEM, allowing the structural stability to be investigated.

SEM was performed using a Jeol JSM 7500F field emission scanning electron microscope (FESEM) and a Zeiss Nvision40 SEM, with accelerating voltage between 2 and 5 kV. Raman and PL were performed using a Renishaw InVia microscope, with a 532 nm laser, for

https://doi.org/10.1021/acsaem.3c03055
ACS Appl. Energy Mater. XXXX, XXX, XXX−XXX

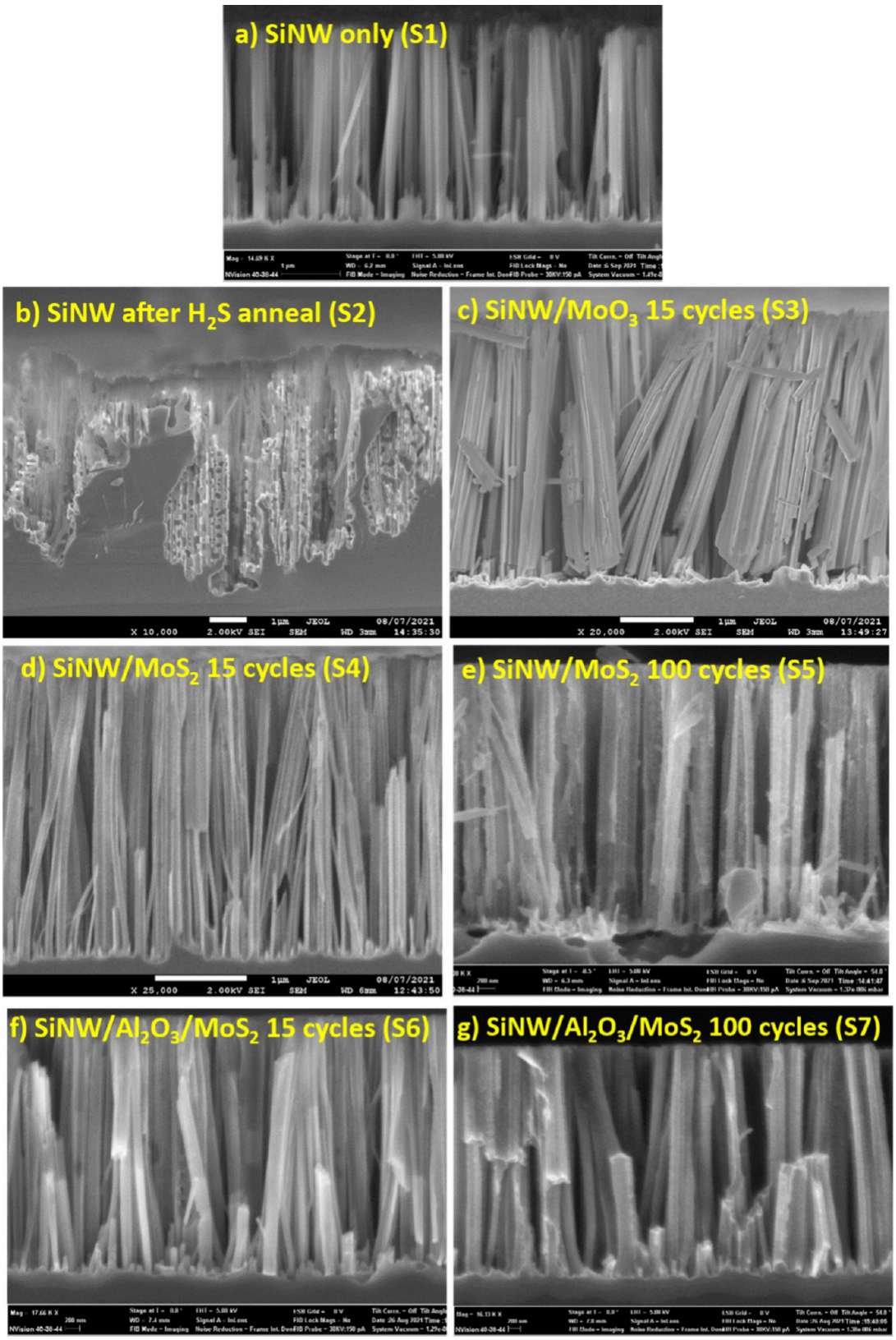

Figure 1. SEM cross-sectional images of SiNWs at different 2D MoS_2 process steps, corresponding to samples from Table 1: (a) reference sample of SiNW with no further processing (S1), (b) SiNW exposed to H_2S anneal with no MoO_3 layer (S2), (c) SiNW with MoO_3 via ALD but no anneal (S3), (d) 15 cycles of MoO_3 ALD followed by H_2S anneal (S4), (e) 100 cycles of MoO_3 followed by H_2S anneal (S5), (f) alumina interface with 15 cycles of MoO_3 ALD followed by H_2S anneal (S6), and (g) alumina interface with 100 cycles of MoO_3 followed by H_2S anneal (S7).

https://doi.org/10.1021/acsaem.3c03055
ACS Appl. Energy Mater. XXXX, XXX, XXX−XXX

10 s irradiation time, with a laser power of 0.55 mW at the sample (1% of 55 mW on sample using a 100 mW laser), at a ×50 objective, for three accumulations per measurement.

Scanning TEM (STEM) micrographs were taken with a Thermo Fisher Scientific (formerly FEI) TEM Titan3 80−300 microscope at 300 kV acceleration voltage. The microscope is equipped with a cs-aberration corrector for the TEM imaging mode. Image acquisition in TEM mode was done with a CCD camera (2k × 2k). STEM micrographs were acquired by using a high-angle annular dark-field (HAADF) detector. Samples were glued into the resin and mechanically polished, followed by ion beam milling for thinning.

RESULTS AND DISCUSSION

SEM. Figure 1 shows the SEM results of the nanowires at varying stages of the fabrication process and for the different splits in the batch, i.e., those with and without alumina, and for two different MoS_2 thicknesses, as determined by the ALD cycle number: 15 and 100. The SEM image (Figure 1(a)) shows the reference sample of SiNWs, with no processing (S1). Figure 1(b) shows the destructive result on silicon nanowires that occurs after the sample is annealed in H_2S when the protective MoO_3 layer is not applied (S2). This demonstrates that H_2S aggressively reacts with Si when exposed directly. It is for this reason that direct growth of MoS_2 onto silicon is incredibly challenging, especially when using traditional CVD processes which directly expose the substrates to H_2S. To overcome this, our two-step MoS_2 process deposits MoO_3 first (Figure 1(c)) (S3), followed by a H_2S anneal. The deposition of the MoO_3 layer first acts as a protection layer to the substrate below, thus facilitating direct growth of MoS_2 onto silicon, with no apparent damage to the nanowire structure below, as shown in Figure 1(d) (S4). This validates the compatibility of using this ALD growth process of MoS_2 with nanowires, based on the nonevident negative effects.

Figure 1(d−g) demonstrates samples S4−S7, respectively, with and without alumina and for the thick and thin MoS_2 layers. While there are no discernible differences between these samples due to the resolution of the SEM, these images still show no structural damage has occurred at any point of our process flow, verifying the fabrication steps are compatible with the SiNWs.

Raman. To confirm successful growth, ascertain the presence of MoS_2 on the silicon nanowires, and measure the number of layers, Raman spectroscopy was performed. Two characteristic MoS_2 peaks, the E_{2g} and A_{1g} at a Raman shift of 380 and 405 cm^{-1}, were seen on all MoS_2 samples (S4 to S7), demonstrating successful growth of MoS_2 on silicon nanowires. Figure 2 is a representative spectrum of all samples with four Raman measurements taken across four spatial locations across the samples. This provided each sample with an average and standard deviation, using a Gaussian fitting function for the peaks.

The Raman peak locations and peak separation of four MoS_2 samples, two with and two without Al_2O_3, with thick and thin layers (S4 to S7) (15 and 100 ALD cycles of MoO_3, converted to MoS_2) are shown in Figure 3. For both samples with 100 cycles of ALD (S5 and S7), a significant increase in peak separation is seen compared with their 15 cycle counterparts (S4 and S6). This increase in peak separation is expected for thicker samples, seen throughout the literature, and can be used to determine the number of layers.[43]

A peak separation of ∼25 cm^{-1} has been reported in the literature to reflect five to six layers[43−45] of MoS_2, with some literature reporting this tends toward "bulk" material behavior.[46−48] This is what we see for the thicker 100 ALD cycle samples in this work.

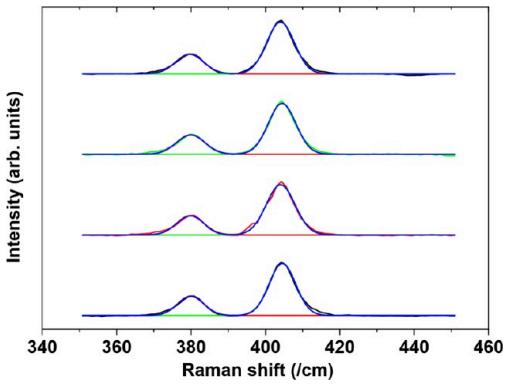

Figure 2. Typical Raman spectra of four points taken on S4 (15 ALD cycles of SiNW/MoS_2), highlighting the MoS_2 lower peak of E_{2g} and the higher peak of A_{1g}.

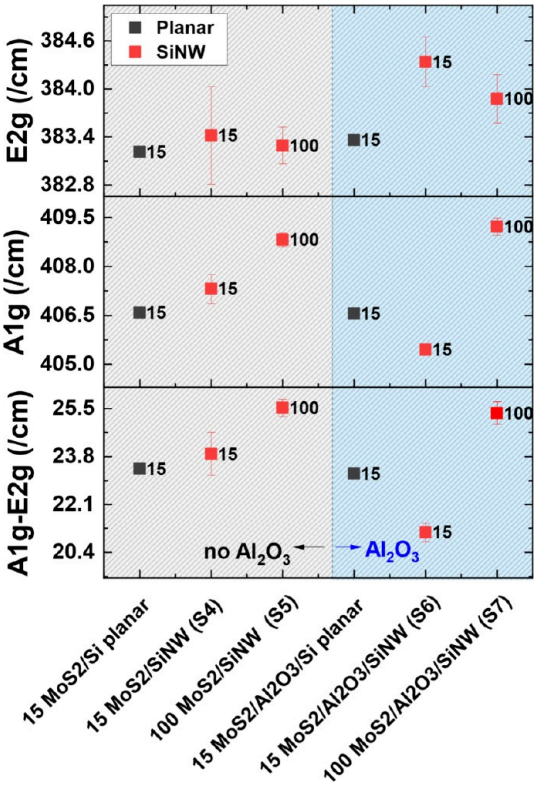

Figure 3. Raman E_{2g} and A_{1g} peak locations, with peak difference shown for SiNW-MoS_2 stacks, with and without alumina for 15 and 100 ALD cycles. A planar reference sample is included.

The 15 cycle ALD samples (S4 and S6) demonstrate a peak separation of ∼24 cm^{-1}, reported to be four MoS_2 layers or below, with SiNW/Al_2O_3/MoS_2 (S6) exhibiting the smallest separation at ∼20 cm^{-1}, indicating one to two layers of MoS_2.[47,49] The presence of Al_2O_3 in combination with the silicon nanowires appears to have resulted in the lowest number of MoS_2 layers. A reason for this could be due to the alumina layer encapsulating the SiNW, acting as a moisture barrier and reducing water and oxygen molecules on the surface of the nanowires. This removal of additional molecules and creating this hydrophilic surface on the SiNWs could therefore remove an interfacial MoO_3 layer that forms when the molybdenum

https://doi.org/10.1021/acsaem.3c03055
ACS Appl. Energy Mater. XXXX, XXX, XXX−XXX

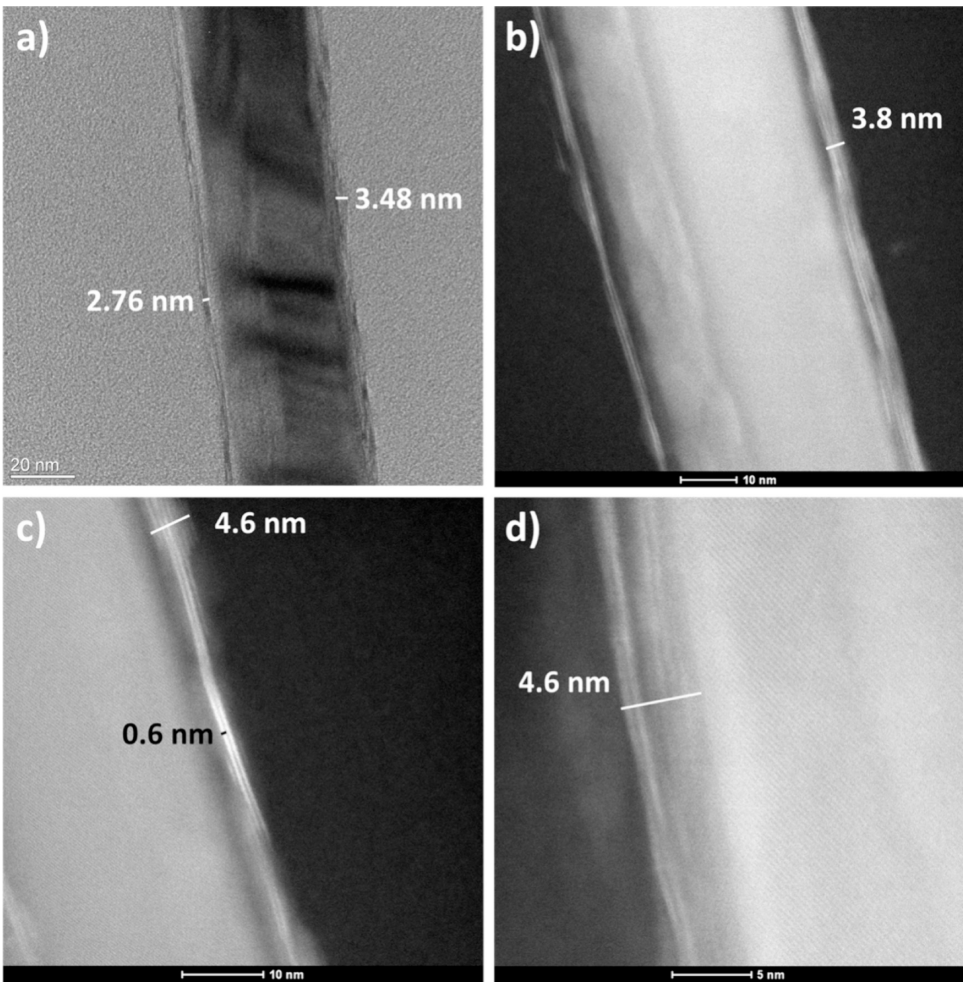

Figure 4. TEM images of nanowire cross sections from a 15 ALD cycles MoS_2/SiNW (S4) sample with no alumina at varying magnifications: (a) ×115k TEM, (b) ×910k scanning TEM, (c) ×1300k scanning TEM, and (d) ×2.55 M scanning TEM. Individual layers of MoS_2 can be seen on the nanowire surface, varying from two layers up to five and above.

precursor first enters the chamber on the first cycle. Where alumina is present and fully reacted, this hydrophilic-terminated surface would mean the first precursor injection does not react with any leftover oxygen and in turn will have a reduced number of subsequent MoO_3 layers.[50]

The presence of MoS_2 Raman peaks occurring across the spatial area of the sample indicates an ability to grow a single layer of MoS_2 conformally on a structured sample across a large area. This, which can be scaled up to 300 mm wafer scales as the standard, is used in semiconductor fabrication plants across the world.[51,52] Furthermore, the ability to directly grow MoS_2 onto bare silicon (15 cycle SiNW/MoS_2), as opposed to growing on silicon dioxide followed by a transfer process, will enable active electronic devices to be processed much more readily and with fewer defects due to the monolithic integration. While Raman has verified a good spatial uniformity at a chip level, TEM was also used to investigate the number of layers for the 15 cycle samples with higher accuracy and determine spatial uniformity across the nanowires and growth orientation.

Transmission Electron Microscopy. TEM was performed on the samples with 15 ALD cycles only (S4 and S6) as these samples will display independent layers, which can be used to confirm Raman results. Figure 4 shows TEM cross sections of a nanowire for the 15 cycle MoS_2/SiNW sample without alumina (S4). The images clearly show continuous parallel MoS_2 coverage over the entire nanowire with between two and five layers. This indicates that there is successful growth along the full surface of the nanowire, matching well with the Raman measurement.

Figure 5 demonstrates TEM images of cross section nanowires from 15 ALD cycles of MoS_2 on SiNWs with alumina (S6). The alumina is clearly present and uniform across the surface of the nanowire, averaging around 15 nm, as expected for this ALD recipe. The MoS_2 layers are clearly present in these images, demonstrating two layers uniformly along the surface of the nanowires. This verifies the Raman results which indicated one to two layers. These TEM images indicate the uniformity and layer number are a lot more consistent across the surface of the nanowires compared to the sample without alumina present, in agreement with Raman results. This indicates that alumina acts as a passivating and seeding layer for higher-quality subsequent MoS_2 growth.

Photoluminescence. To confirm the presence of monolayers and ascertain the layer film quality, photoluminescence measurements were performed. The raw data of the four SiNW/MoS_2 samples can be seen in Figure 6, whereby the photoluminescence intensity is plotted. The normalized PL plot for the samples is shown in Figure 7, normalized by the maximum intensity, and fitted with three Gaussian peaks that correspond to the peaks seen in typical MoS_2 PL spectra.[53] The

https://doi.org/10.1021/acsaem.3c03055
ACS Appl. Energy Mater. XXXX, XXX, XXX−XXX

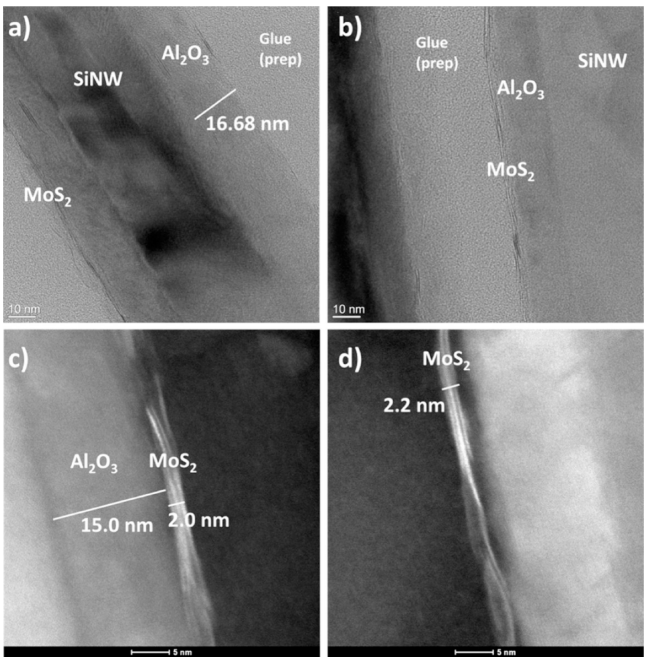

Figure 5. TEM images of nanowire cross sections from a 15 ALD cycles MoS_2/Al_2O_3/SiNW (S) sample with alumina at varying magnifications: (a) ×45k TEM, (b) ×145k TEM, (c) ×1.8 M scanning TEM, and (d) ×1.8 M scanning TEM. A uniform alumina layer is visible with two layers of MoS_2 distributed uniformly across the nanowire surface.

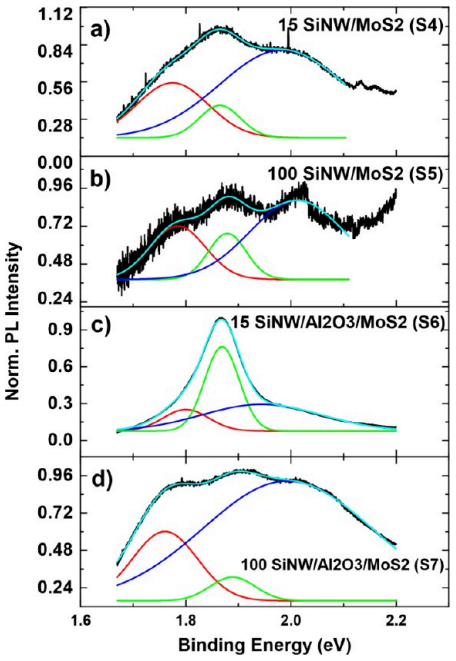

Figure 7. Normalized and fitted photoluminescence peaks of SiNW-MoS_2 stacks for (a) 15 cycles of MoS_2 without alumina (S4), (b) 100 cycles of MoS_2 without alumina (S5), (c) 15 cycles of MoS_2 with alumina (S6), and (d) 100 cycles of MoS_2 with alumina (S7).

green middle peak is the A exciton; the blue highest energy peak is the B exciton; while the red lowest-energy peak is identified as

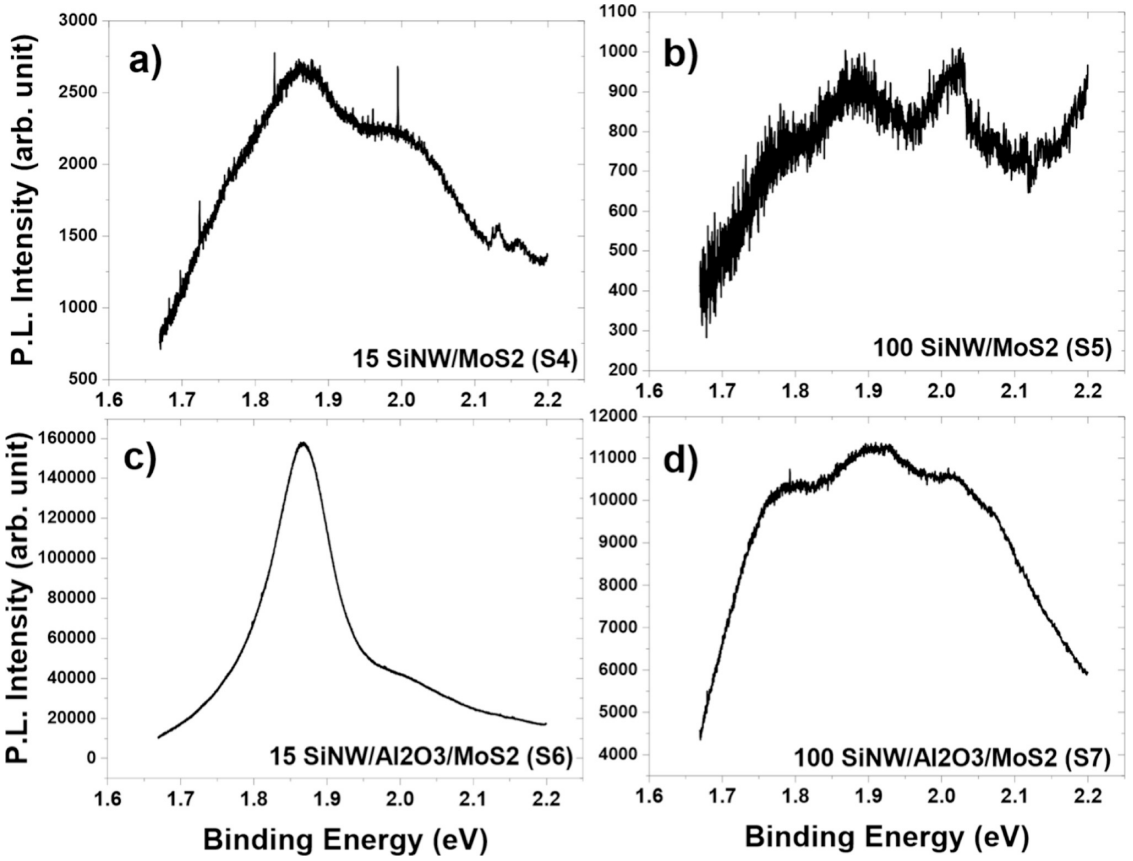

Figure 6. Raw photoluminescence data for SiNW-MoS_2 samples, with measured intensity, for (a) 15 cycles of MoS_2 without alumina (S4), (b) 100 cycles of MoS_2 without alumina (S5), (c) 15 cycles of MoS_2 with alumina (S6), and (d) 100 cycles of MoS_2 with alumina (S7).

https://doi.org/10.1021/acsaem.3c03055
ACS Appl. Energy Mater. XXXX, XXX, XXX−XXX

the A-Trion, often related to the presence of defects, doping, or substrate effects causing excess electron charges.[53]

The 15 cycle SiNW/Al_2O_3/MoS_2 sample (S6) exhibits typical monolayer MoS_2 PL spectra often seen in the literature, with a dominant A exciton peak at 1.87 eV and a small A-Trion and B exciton peak at 1.84 and 1.96 eV, respectively, and a B/A intensity ratio of 0.3.[54−56] The higher absolute intensity of this sample compared to the others, as seen in Figure 6, might also indicate the presence of a stronger PL, indicating fewer MoS_2 layers are present in comparison to the other samples as also shown through the TEM. The 15 cycle SiNW/MoS_2 (S4) sample also exhibits the MoS_2 peak shape as seen in the literature, although the high B/A peak intensity of nearly 3 indicates a higher defect density and thus lower MoS_2 quality.[57] This would suggest that the alumina layer promotes a better quality subsequent MoS_2 film.

The 100 cycle samples (S5 and S7) exhibit a lower absolute intensity, which could be attributed to bulk-type behavior where an indirect band gap is present, rather than a direct one as for monolayer samples, thus losing the emergence of strong photoluminescence. Nonetheless, the B/A ratio is better for the 100-cycle sample without alumina (S5), at 1.7, than for the sample with alumina (S7), at 5.0, which indicates a reduction in MoS_2 quality conferred by the alumina buffer for the thicker MoS_2. This could be due to the alumina creating a better interfacial layer for the subsequent MoO_3 growth, which is more prominent when the layers are thin but is dwarfed in thicker samples. In addition, the alumina layer could act as a protective layer for the silicon against the H_2S anneal for the thin MoO_3 samples, but this effect is unnecessary when the thicker MoO_3 layer acts as a protective layer itself.

The trion peak is present in all four samples, indicating a typical excess of electrons as commonly reported in the literature for MoS_2.[55,58,59] The absolute intensity of the A-Trion peak is largest for the 100 cycles with alumina (S7) but is then followed by the 15 cycles without alumina (S4), with the smallest intensity coming from the 15 cycles with alumina (S6). Therefore, there does not appear to be a clear trend with Trion peak intensity and the substrate and cycle number.

The reduction in the A exciton intensity, along with the red-shifted and larger intensity A-Trion peak, has been reported in the literature for samples that are n-type.[60,61] These features can be seen for both the 100 cycle samples (S5 and S7) and the 15 cycles without alumina (S4), when compared with the 15 cycles with alumina (S6).

We can conclude that the 15 cycles of ALD MoS_2 with alumina (S6), with the highest PL A exciton peak intensity and lowest B/A peak intensity ratio, along with a nonredshifted and lower intensity A-Trion peak, demonstrate the sample with the least number of excess electrons and unintentional n-type doping and thus have the highest-quality MoS_2. For the thickest samples, the opposite trend with alumina is seen. Therefore, the use of an alumina layer can be selected depending on the ideal thickness required for the specific application and whether an insulating layer is plausible. For example, if used as an electrode in an ion battery application, it may be better to have many layers so that a higher number of ions can be inserted, thus increasing battery capacity. As such, our results would indicate an alumina layer is not necessary for higher-layer numbers, as a better quality MoS_2 is seen for thicker films directly grown onto SiNWs, which will also allow for the silicon to contribute higher electrical conductivity, potentially further enhancing battery performance. However, if MoS_2 is to be used as a standalone layer that is to be electrically isolated from the substrate, a better quality fewer-layer MoS_2 film could be achieved with an underlining alumina layer present. A stack such as this, with large surface area MoS_2, would be an ideal electrolyte−electrode interfacial layer to promote ion insertion or photocathodes for water splitting, leading toward renewable solar-powered hydrogen fuel generation,[21] or for highly sensitive gas sensing for pollution and environmental monitoring.[22]

FUTURE WORK/BATTERY DEVICES

The heterostructures discussed here have potential to be used as battery electrodes with ion intercalation and deintercalation occurring between the MoS_2 layers. Future work to demonstrate the performance of the heterostructure will include creating a pouch cell assembly, with the nanowire/2D heterostructures on the silicon substrate acting as a standalone electrode. Cyclic voltammetry and galvanostatic charge/discharge tests will be used to define the ionic mechanisms and specific capacity of the electrode which will be compared to other materials such as graphite. Beyond lithium ions, aluminum and sodium chemistry will be used to explore more environmentally and readily available ion battery technologies. Further investigations using flexible textured substrates will also be performed, for the application of flexible 2D batteries, as 2D materials are inherently flexible in their very nature.

CONCLUSIONS

2D MoS_2/SiNW heterostructures were fabricated, with MoS_2 layer numbers tuned through control of the ALD cycle number, using a large-area, commercially scalable, two-step ALD/H_2S anneal process. ALD alumina was used as an interfacial layer between MoS_2 and nanowires. SEM verified that this two-step process results in no degradation of the silicon nanowires, whereby the MoO_3 layer grown first protects the silicon from the H_2S gas during anneal, while also allowing for the MoO_3 to be converted to MoS_2. The 100 ALD cycle samples demonstrate near bulk behavior by Raman with a peak separation of ∼25 cm^{-1} and show the lowest intensity in photoluminescence. The 15 ALD cycle samples demonstrated one to four MoS_2 layers, with the presence of alumina reducing the Raman peak separation to 20 cm^{-1}, indicating near monolayer growth. This was confirmed with TEM, where parallel growth is shown conformally across the silicon nanowire surface with two layers present. Photoluminescence demonstrated that the quality of the 15 ALD cycle samples is significantly improved in terms of defects, with a reduction in B/A intensity from 3 to 0.3. This work demonstrates a commercially compatible MoS_2/SiNW heterostructure technique that is highly controllable and adaptable, allowing for substrate choice with or without an insulator, along with number of layers to be selected, lending the systems unique properties to applications in the energy storage and generation space.

ASSOCIATED CONTENT

Data Availability Statement

The data that support the findings of this study are available in 10.5258/SOTON/D2829

AUTHOR INFORMATION

Corresponding Author

Katrina A. Morgan − *Electronics and Computer Science, University of Southampton, Southampton SO171BJ, U.K.;*

https://doi.org/10.1021/acsaem.3c03055
ACS Appl. Energy Mater. XXXX, XXX, XXX−XXX

orcid.org/0000-0002-8600-4322; Email: kam2g11@soton.ac.uk

Authors

Ioannis Zeimpekis − *Electronics and Computer Science, University of Southampton, Southampton SO171BJ, U.K.*

Tasmiat Rahman − *Electronics and Computer Science, University of Southampton, Southampton SO171BJ, U.K.*

Oi Man Leung − *Faculty of Engineering and Physical Sciences, Mechanical Engineering department, University of Southampton, Southampton SO171BJ, U.K.;* orcid.org/0000-0002-1951-6811

Jack Tyson − *Electronics and Computer Science, University of Southampton, Southampton SO171BJ, U.K.*

Martin Ebert − *Electronics and Computer Science, University of Southampton, Southampton SO171BJ, U.K.*

Stuart A. Boden − *Electronics and Computer Science, University of Southampton, Southampton SO171BJ, U.K.*

Carlos Ponce De Leon − *Faculty of Engineering and Physical Sciences, Mechanical Engineering department, University of Southampton, Southampton SO171BJ, U.K.*

Complete contact information is available at: https://pubs.acs.org/10.1021/acsaem.3c03055

Author Contributions

The manuscript was written by K. A. Morgan and I. Zeimpekis, with all authors editing the manuscript. The project was conceptualized by T. Rahman and K. A. Morgan. The funding and project were secured and managed by K. A. Morgan as principal investigator and T. Rahman and I. Zeimpekis as coinvestigators, along with the design of experiments and design of analysis. Samples were fabricated by J. Tyson and K. A. Morgan. The data was collected by S. Z. Oo, O. M. Leung, M. Ebert, and K. A. Morgan. The analysis of the data was performed by K. A. Morgan, I. Zeimpekis, T. Rahman, O. M. Leung, S. Boden, and C. Ponce de Leon Albarran.

Funding

The work in this paper is supported by the Engineering and Physical Sciences Research Council (EPSRC) in part through Grant EP/X016730/1, Smart Cloth—a wearable system powered entirely by body heat, Grant EP/M015130/1, Manufacturing and Application of Next Generation Chalcogenides, and Grant EP/W022931/1A— Photonic−Electronic nonvon Neumann Processor Core for Highly Efficient Computing (APT-NuCOM). O.M.L. acknowledges funding from the Lloyd's Register Foundation International Consortium of Nanotechnologies [G0086]. Finally, this work was supported by the Zepler Institute Stimulus Fund at the University of Southampton, which is supported by HEFCE's Higher Education Innovation Fund (HEIF), awarded to the University to help foster collaborations with industry and other users of research.

Notes

The authors declare no competing financial interest.

■ ACKNOWLEDGMENTS

Christian Patzig from Fraunhofer Institute for Microstructure of Materials and Systems IMWS is acknowledged for performing the TEM sample preparation and measurements.

■ REFERENCES

(1) Singh, M.; Das, P.; Samanta, P. N.; Bera, S.; Thantirige, R.; Shook, B.; Nejat, R.; Behera, B.; Zhang, Q.; Dai, Q.; Pramanik, A.; Ray, P.; Raghavan, D.; Leszczynski, J.; Karim, A.; Pradhan, N. R. Ultrahigh Capacitive Energy Density in Stratified 2D Nanofiller-Based Polymer Dielectric Films. *ACS Nano* **2023**, *17*, 20262.

(2) Cai, C.; Tao, Z.; Zhu, Y.; Tan, Y.; Wang, A.; Zhou, H.; Yang, Y. A nano interlayer spacing and rich defect 1T-MoS2 as cathode for superior performance aqueous zinc-ion batteries. *Nanoscale Adv.* **2021**, *3* (13), 3780−3787.

(3) Han, M.; Mu, Y.; Guo, J.; Wei, L.; Zeng, L.; Zhao, T. Monolayer MoS2 Fabricated by In Situ Construction of Interlayer Electrostatic Repulsion Enables Ultrafast Ion Transport in Lithium-Ion Batteries. *Nano-Micro Letters* **2023**, *15* (1), 80.

(4) Rasamani, K. D.; Alimohammadi, F.; Sun, Y. Interlayer-expanded MoS2. *Mater. Today* **2017**, *20* (2), 83−91.

(5) Wang, L.; Zhang, X.; Xu, Y.; Li, C.; Liu, W.; Yi, S.; Wang, K.; Sun, X.; Wu, Z.-S.; Ma, Y. Tetrabutylammonium-Intercalated 1T-MoS2 Nanosheets with Expanded Interlayer Spacing Vertically Coupled on 2D Delaminated MXene for High-Performance Lithium-Ion Capacitors. *Adv. Funct. Mater.* **2021**, *31* (36), No. 2104286.

(6) Sarkar, D.; Das, D.; Das, S.; Kumar, A.; Patil, S.; Nanda, K. K.; Sarma, D. D.; Shukla, A. Expanding Interlayer Spacing in MoS2 for Realizing an Advanced Supercapacitor. *ACS Energy Lett.* **2019**, *4* (7), 1602−1609.

(7) Li, Y.; Liang, Y.; Robles Hernandez, F. C.; Deog Yoo, H.; An, Q.; Yao, Y. Enhancing sodium-ion battery performance with interlayer-expanded MoS2−PEO nanocomposites. *Nano Energy* **2015**, *15*, 453−461.

(8) Stephenson, T.; Li, Z.; Olsen, B.; Mitlin, D. Lithium ion battery applications of molybdenum disulfide (MoS2) nanocomposites. *Energy Environ. Sci.* **2014**, *7* (1), 209−231.

(9) Li, Z.; Sami, I.; Yang, J.; Li, J.; Kumar, R. V.; Chhowalla, M. Lithiated metallic molybdenum disulfide nanosheets for high-performance lithium−sulfur batteries. *Nature Energy* **2023**, *8* (1), 84−93.

(10) Majidi, L.; Yasaei, P.; Warburton, R. E.; Fuladi, S.; Cavin, J.; Hu, X.; Hemmat, Z.; Cho, S. B.; Abbasi, P.; Vörös, M.; Cheng, L.; Sayahpour, B.; Bolotin, I. L.; Zapol, P.; Greeley, J.; Klie, R. F.; Mishra, R.; Khalili-Araghi, F.; Curtiss, L. A.; Salehi-Khojin, A. New Class of Electrocatalysts Based on 2D Transition Metal Dichalcogenides in Ionic Liquid. *Adv. Mater.* **2019**, *31* (4), No. 1804453.

(11) Samy, O.; El Moutaouakil, A. A Review on MoS2 Energy Applications: Recent Developments and Challenges. *Energies* **2021**, *14* (15), 4586.

(12) Kim, S.; Lee, Y. M. Two-dimensional nanosheets and membranes for their emerging technologies. *Current Opinion in Chemical Engineering* **2023**, *39*, No. 100893.

(13) Li, H.; Zhang, W. Perovskite Tandem Solar Cells: From Fundamentals to Commercial Deployment. *Chem. Rev.* **2020**, *120* (18), 9835−9950.

(14) Kim, E.-B.; Akhtar, M. S.; Shin, H.-S.; Ameen, S.; Nazeeruddin, M. K. A review on two-dimensional (2D) and 2D-3D multidimensional perovskite solar cells: Perovskites structures, stability, and photovoltaic performances. *Journal of Photochemistry and Photobiology C: Photochemistry Reviews* **2021**, *48*, No. 100405.

(15) Lin, S.; Li, X.; Wang, P.; Xu, Z.; Zhang, S.; Zhong, H.; Wu, Z.; Xu, W.; Chen, H. Interface designed MoS2/GaAs heterostructure solar cell with sandwich stacked hexagonal boron nitride. *Sci. Rep.* **2015**, *5* (1), 15103.

(16) Singh, R.; Giri, A.; Pal, M.; Thiyagarajan, K.; Kwak, J.; Lee, J.-J.; Jeong, U.; Cho, K. Perovskite solar cells with an MoS 2 electron transport layer. *Journal of Materials Chemistry A* **2019**, *7* (12), 7151−7158.

(17) He, Z.; Que, W. Molybdenum disulfide nanomaterials: Structures, properties, synthesis and recent progress on hydrogen evolution reaction. *Appl. Mater. Today* **2016**, *3*, 23−56.

(18) Yang, L.; Liu, P.; Li, J.; Xiang, B. Two-dimensional material molybdenum disulfides as electrocatalysts for hydrogen evolution. *Catalysts* **2017**, *7* (10), 285.

(19) Chen, Z.; Cummins, D.; Reinecke, B. N.; Clark, E.; Sunkara, M. K.; Jaramillo, T. F. Core−shell MoO3−MoS2 Nanowires for Hydrogen Evolution: A Functional Design for Electrocatalytic Materials. *Nano Lett.* **2011**, *11* (10), 4168−4175.
(20) Mao, J.; Zhang, B.; Shi, Y.; Wu, X.; He, Y.; Wu, D.; Jie, J.; Lee, C. S.; Zhang, X. Conformal MoS2/silicon nanowire array heterojunction with enhanced light trapping and effective interface passivation for ultraweak infrared light detection. *Adv. Funct. Mater.* **2022**, *32* (11), No. 2108174.
(21) Zhang, L.; Liu, C.; Wong, A. B.; Resasco, J.; Yang, P. MoS 2-wrapped silicon nanowires for photoelectrochemical water reduction. *Nano Research* **2015**, *8*, 281−287.
(22) Zhao, S.; Li, Z.; Wang, G.; Liao, J.; Lv, S.; Zhu, Z. Highly enhanced response of MoS 2/porous silicon nanowire heterojunctions to NO 2 at room temperature. *RSC Adv.* **2018**, *8* (20), 11070−11077.
(23) Choudhary, N.; Park, J.; Hwang, J. Y.; Choi, W. Growth of large-scale and thickness-modulated MoS2 nanosheets. *ACS Appl. Mater. Interfaces* **2014**, *6* (23), 21215−21222.
(24) Hussain, S.; Singh, J.; Vikraman, D.; Singh, A. K.; Iqbal, M. Z.; Khan, M. F.; Kumar, P.; Choi, D.-C.; Song, W.; An, K.-S.; et al. Large-area, continuous and high electrical performances of bilayer to few layers MoS2 fabricated by RF sputtering via post-deposition annealing method. *Sci. Rep.* **2016**, *6* (1), 30791.
(25) Abbas, O. A.; Lewis, A. H.; Aspiotis, N.; Huang, C.-C.; Zeimpekis, I.; Hewak, D. W.; Sazio, P.; Mailis, S. Laser printed two-dimensional transition metal dichalcogenides. *Sci. Rep.* **2021**, *11* (1), 5211.
(26) Abbas, O. A.; Zeimpekis, I.; Wang, H.; Lewis, A. H.; Sessions, N. P.; Ebert, M.; Aspiotis, N.; Huang, C.-C.; Hewak, D.; Mailis, S.; et al. Solution-based synthesis of few-layer WS2 large area continuous films for electronic applications. *Sci. Rep.* **2020**, *10* (1), 1696.
(27) Hossain, R. F.; Deaguero, I. G.; Boland, T.; Kaul, A. B. Biocompatible, large-format, inkjet printed heterostructure MoS2-graphene photodetectors on conformable substrates. *npj 2D Mater. Appl.* **2017**, *1* (1), 28.
(28) Seo, J.-W. T.; Zhu, J.; Sangwan, V. K.; Secor, E. B.; Wallace, S. G.; Hersam, M. C. Fully inkjet-printed, mechanically flexible MoS2 nanosheet photodetectors. *ACS Appl. Mater. Interfaces* **2019**, *11* (6), 5675−5681.
(29) Wan, X.; Miao, X.; Yao, J.; Wang, S.; Shao, F.; Xiao, S.; Zhan, R.; Chen, K.; Zeng, X.; Gu, X.; Xu, J. In Situ Ultrafast and Patterned Growth of Transition Metal Dichalcogenides from Inkjet-Printed Aqueous Precursors. *Adv. Mater.* **2021**, *33* (16), No. 2100260.
(30) Huang, C.-C.; Al-Saab, F.; Wang, Y.; Ou, J.-Y.; Walker, J. C.; Wang, S.; Gholipour, B.; Simpson, R. E.; Hewak, D. W. Scalable high-mobility MoS 2 thin films fabricated by an atmospheric pressure chemical vapor deposition process at ambient temperature. *Nanoscale* **2014**, *6* (21), 12792−12797.
(31) Schmidt, H.; Wang, S.; Chu, L.; Toh, M.; Kumar, R.; Zhao, W.; Castro Neto, A.; Martin, J.; Adam, S.; Özyilmaz, B.; et al. Transport properties of monolayer MoS2 grown by chemical vapor deposition. *Nano Lett.* **2014**, *14* (4), 1909−1913.
(32) Wu, W.; De, D.; Chang, S.-C.; Wang, Y.; Peng, H.; Bao, J.; Pei, S.-S. High mobility and high on/off ratio field-effect transistors based on chemical vapor deposited single-crystal MoS2 grains. *Appl. Phys. Lett.* **2013**, DOI: 10.1063/1.4801861.
(33) Jang, Y.; Yeo, S.; Lee, H.-B.-R.; Kim, H.; Kim, S.-H. Wafer-scale, conformal and direct growth of MoS2 thin films by atomic layer deposition. *Appl. Surf. Sci.* **2016**, *365*, 160−165.
(34) Kheng, T. L.; Bo, L.; Hua, T. J. Atomic Layer Deposition of a MoS2 Film. *Nanoscale* **2014**, *6*, 10584−10588.
(35) Shi, Y.; Li, H.; Li, L.-J. Recent advances in controlled synthesis of two-dimensional transition metal dichalcogenides via vapour deposition techniques. *Chem. Soc. Rev.* **2015**, *44* (9), 2744−2756.
(36) Rahman, T.; Bonilla, R. S.; Nawabjan, A.; Wilshaw, P. R.; Boden, S. A. Passivation of all-angle black surfaces for silicon solar cells. *Sol. Energy Mater. Sol. Cells* **2017**, *160*, 444−453.
(37) Scheul, T.; Khorani, E.; Rahman, T.; Boden, S. Metal-assisted chemically etched black silicon for crystalline silicon solar cells. Presented at the *PV-SAT 14*; Imperial College London: London, United Kingdom, 18th-20th April, 2018.
(38) Scheul, T. E. Metal-assisted chemically etched black silicon: morphology and light interaction. *PhD*, University of Southampton, https://eprints.soton.ac.uk/448519/, 2020.
(39) Aspiotis, N.; Morgan, K.; März, B.; Müller-Caspary, K.; Ebert, M.; Weatherby, E.; Light, M. E.; Huang, C.-C.; Hewak, D. W.; Majumdar, S.; Zeimpekis, I. Large-area synthesis of high electrical performance MoS2 by a commercially scalable atomic layer deposition process. *npj 2D Mater. Appl.* **2023**, *7* (1), 18.
(40) Scheul, T. E.; Khorani, E.; Rahman, T.; Boden, S. A. Characterization of atomic layer deposited alumina thin films on black silicon textures using helium ion microscopy. *AIP Conf. Proc.* **2019**, DOI: 10.1063/1.5123858.
(41) Gullapalli, H.; Kalaga, K.; Vinod, S.; Rodrigues, M.-T. F.; George, A.; Ajayan, P. M. 2D material integrated macroporous electrodes for Li-ion batteries. *Rsc Advances* **2017**, *7* (52), 32737−32742.
(42) Peng, L.; Zhu, Y.; Chen, D.; Ruoff, R. S.; Yu, G. Two-dimensional materials for beyond-lithium-ion batteries. *Adv. Energy Mater.* **2016**, *6* (11), No. 1600025.
(43) Plechinger, G.; Heydrich, S.; Eroms, J.; Weiss, D.; Schüller, C.; Korn, T. Raman spectroscopy of the interlayer shear mode in few-layer MoS2 flakes. *Appl. Phys. Lett.* **2012**, DOI: 10.1063/1.4751266.
(44) Jin, K.; Liu, D.; Tian, Y. Enhancing the interlayer adhesive force in twisted multilayer MoS2 by thermal annealing treatment. *Nanotechnology* **2015**, *26* (40), No. 405708.
(45) Niu, Y.; Gonzalez-Abad, S.; Frisenda, R.; Marauhn, P.; Drüppel, M.; Gant, P.; Schmidt, R.; Taghavi, N. S.; Barcons, D.; Molina-Mendoza, A. J.; et al. Thickness-dependent differential reflectance spectra of monolayer and few-layer MoS2, MoSe2, WS2 and WSe2. *Nanomaterials* **2018**, *8* (9), 725.
(46) Ostrikov, K.; Gu, X.; Han, Z. J.; Ni, Z.; Qin, F.; Xiao, P.; Xiao, S.; Yan, D.; Zhang, X. Atomic-layer soft plasma etching of MoS2. *Sci. Rep.* **2016**, DOI: 10.1038/srep19945.
(47) Ye, M.; Winslow, D.; Zhang, D.; Pandey, R.; Yap, Y. K. Recent advancement on the optical properties of two-dimensional molybdenum disulfide (MoS2) thin films. In *Photonics*; MDPI, 2015; Vol. *2*, no. 1, pp 288−307.
(48) Yuan, P.; Li, C.; Xu, S.; Liu, J.; Wang, X. Interfacial thermal conductance between few to tens of layered-MoS2 and c-Si: Effect of MoS2 thickness. *Acta Mater.* **2017**, *122*, 152−165.
(49) Xiao, S.; Xiao, P.; Zhang, X.; Yan, D.; Gu, X.; Qin, F.; Ni, Z.; Han, Z. J.; Ostrikov, K. Atomic-layer soft plasma etching of MoS2. *Sci. Rep.* **2016**, *6* (1), No. 19945.
(50) Han, P.; Adler, E. R.; Liu, Y.; St Marie, L.; El Fatimy, A.; Melis, S.; Van Keuren, E.; Barbara, P. Ambient effects on photogating in MoS2 photodetectors. *Nanotechnology* **2019**, *30* (28), No. 284004.
(51) Smets, Q.; Schram, T.; Verreck, D.; Cott, D.; Groven, B.; Ahmed, Z.; Kaczer, B.; Mitard, J.; Wu, X.; Kundu, S.; Mertens, H.; Radisic, D.; Thiam, A.; Li, W.; Dupuy, E.; Tao, Z.; Vandersmissen, K.; Maurice, T.; Lin, D.; Morin, P.; Asselberghs, I.; Radu, I. Scaling of double-gated WS2 FETs to sub-5nm physical gate length fabricated in a 300mm FAB. *2021 IEEE International Electron Devices Meeting (IEDM)* **2021**, 34.2.1−34.2.4.
(52) Xia, Y.; Chen, X.; Wei, J.; Wang, S.; Chen, S.; Wu, S.; Ji, M.; Sun, Z.; Xu, Z.; Bao, W.; Zhou, P. 12-in. growth of uniform MoS2 monolayer for integrated circuit manufacture. *Nat. Mater.* **2023**, *22* (11), 1324−1331.
(53) Goswami, T.; Rani, R.; Hazra, K. S.; Ghosh, H. N. Ultrafast carrier dynamics of the exciton and trion in MoS2 monolayers followed by dissociation dynamics in Au@ MoS2 2D heterointerfaces. *journal of physical chemistry letters* **2019**, *10* (11), 3057−3063.
(54) Kaplan, D.; Gong, Y.; Mills, K.; Swaminathan, V.; Ajayan, P.; Shirodkar, S.; Kaxiras, E. Excitation intensity dependence of photoluminescence from monolayers of MoS2 and WS2/MoS2 heterostructures. *2D Materials* **2016**, *3* (1), No. 015005.
(55) Golovynskyi, S.; Irfan, I.; Bosi, M.; Seravalli, L.; Datsenko, O. I.; Golovynska, I.; Li, B.; Lin, D.; Qu, J. Exciton and trion in few-layer

https://doi.org/10.1021/acsaem.3c03055
ACS Appl. Energy Mater. XXXX, XXX, XXX−XXX

MoS2: Thickness- and temperature-dependent photoluminescence. *Appl. Surf. Sci.* **2020**, *515*, No. 146033.
(56) Mouri, S.; Miyauchi, Y.; Matsuda, K. Tunable Photoluminescence of Monolayer MoS2 via Chemical Doping. *Nano Lett.* **2013**, *13* (12), 5944−5948.
(57) McCreary, K. M.; Hanbicki, A. T.; Sivaram, S. V.; Jonker, B. T. A- and B-exciton photoluminescence intensity ratio as a measure of sample quality for transition metal dichalcogenide monolayers. *Appl Materials* **2018**, DOI: 10.1063/1.5053699.
(58) Christopher, J. W.; Goldberg, B. B.; Swan, A. K. Long tailed trions in monolayer MoS2: Temperature dependent asymmetry and resulting red-shift of trion photoluminescence spectra. *Sci. Rep.* **2017**, *7* (1), 14062.
(59) Li, J.; Ji, Q.; Chu, S.; Zhang, Y.; Li, Y.; Gong, Q.; Liu, K.; Shi, K. Tuning the photo-response in monolayer MoS2 by plasmonic nano-antenna. *Sci. Rep.* **2016**, *6* (1), 23626.
(60) Zhumagulov, Y. V.; Vagov, A.; Gulevich, D. R.; Faria Junior, P. E.; Perebeinos, V. Trion induced photoluminescence of a doped MoS2 monolayer. *J. Chem. Phys.* **2020**, DOI: 10.1063/5.0012971.
(61) Mak, K. F.; He, K.; Lee, C.; Lee, G. H.; Hone, J.; Heinz, T. F.; Shan, J. Tightly bound trions in monolayer MoS2. *Nat. Mater.* **2013**, *12* (3), 207−211.

https://doi.org/10.1021/acsaem.3c03055
ACS Appl. Energy Mater. XXXX, XXX, XXX−XXX